

Production of reactive species by atmospheric pressure streamers in N₂–O₂ mixtures*

Milan Šimek[‡], Martin Člupek, Václav Babický, and Pavel Šunka

Institute of Plasma Physics, Department of Pulse Plasma Systems, Academy of Sciences of the Czech Republic, Za Slovankou 3, 18200 Prague 8, Czech Republic

Abstract: Streamer discharges in atmospheric gases are currently receiving increased attention in connection with environmental issues or new material treatment technologies. The chemical reactivity of streamer-produced plasma, created by various active atomic and molecular species, is a critical parameter for most application areas. Recently, advanced diagnostics based on optical and energy transfer methods have been applied to study dynamics and spatial distribution of several important streamer-produced species. This paper presents an overview of the most recently reported experimental achievements to monitor and detect reactive species, such as, e.g., NO, OH, and O₃ radicals, nitrogen and oxygen atoms, or N₂(A³Σ) metastables.

Keywords: streamers; discharge; corona; LIF; energy pooling; TALIF; OODR-LIF.

INTRODUCTION

A filamentary streamer is a rather frequent form of high-pressure transient discharge which develops from an electron avalanche in an overvolted gap [1–3]. The most important streamer characteristics are very high propagation velocity, a small streamer channel radius, and high density and mean energy of free electrons occurring in the streamer head. Streamers are usually produced in the gas phase between metallic electrodes in high-voltage (HV) systems. Nevertheless, they may also occur between electrodes fully or partially covered with a dielectric barrier [4], on the interface between gaseous and liquid phases [5], and they may even be produced in liquids [6,7].

Various streamer-based discharges in atmospheric gases have currently become hot topics in connection with environmental issues (e.g., air pollution control or ozone synthesis), material treatment technologies (e.g., surface modification and hardening), and biomedical applications (e.g., sterilization or treatment of living tissues) [8–16]. The main reason for increased attention to these topics is the limited efficiency of conventional pollution control technologies (such as carbon adsorption and catalytic/thermal oxidation) and the incompatibility of vacuum-based low-pressure plasma treatment techniques with industrial process lines (such as surface modification of polymers or surface hardening of ferrous metals). The most important issue for such applications is the requirement to optimize efficiency and scale up laboratory devices so as to achieve maximum performance at minimal cost.

As the physics of streamers is still not well understood, advanced experiments, together with physical and chemical modeling, are therefore necessary. Kinetic schemes describing physicochemical phenomena induced by streamers are far from being complete, and the rate constants of individual ele-

*Paper presented at the 17th International Symposium on Plasma Chemistry (ISPC 17), Toronto, Ontario, Canada, 7–12 August 2005. Other presentations are published in this issue, pp. 1093–1298.

[‡]Corresponding author

mentary reactions are known, in many cases, with considerable uncertainty [17–21]. Consequently, currently used numerical codes are based on many assumptions and estimates [22–27].

Traditional and well-established diagnostics that have been used to investigate streamers (e.g., cloud chamber tracks, streak pictures, fast photography, Schlieren photography, emission spectroscopy, and electrical measurements) provided useful information on some fundamentals (e.g., avalanche-streamer formation, streamer propagation and branching, gas and electron temperatures) [28–35]. Information on many other important physical and chemical processes determining streamer properties (e.g., photoionization and recombination, diffusion, vibrational relaxation, streamer channel heating and expansion, production and quenching of atoms, molecular metastable species, and radicals) is, however, very incomplete [36–39]. Given this situation, any new or improved experimental measurements of streamer properties could well be a significant step for further progress.

GENERATION OF STREAMER DISCHARGES

The process of avalanche-to-streamer transition and subsequent streamer propagation requires a sufficiently large external electric field. Suitable conditions can be easily obtained by applying DC, AC, or pulsed HV power in non-uniform electrode configurations (e.g., point-plane, wire-plane, wire-cylinder) [40]. Systems based on DC/AC power usually produce streamers distributed randomly in time and space around an HV electrode and, as a rule, must be protected against streamer-to-spark transition. Sparking in the DC/AC system may be prevented by limiting appropriately the discharge current, e.g., by means of dielectric barriers separating electrodes, resistors in an external electrical circuit, fast gas flow, etc. Providing a sufficiently short duration of the applied HV waveform, pulsed systems are, in comparison with DC/AC generators, intrinsically sparking-free, therefore, they can operate with much higher electric fields. One can expect that a higher electric field will likely produce electrons with higher energies, which may result in higher rates of induced plasma-chemical reactions. Moreover, providing a fast rise time of applied HV pulse, large numbers of streamers can be generated simultaneously. Pulsed systems are, therefore, predestined to produce large-volume and high streamer density plasmas.

Actually, a significant drawback of pulsed systems [41,42] is the complexity and cost of the HV pulsed power supplies compared with that of the DC/AC. Positive voltage polarity is applied mostly to the HV electrode. A typical HV power supply consists of an HV DC power supply, an energy storage element, and a fast switch. Usually, well-developed, low-inductance capacitors or pulse-forming lines are used as energy storage elements. The main problem in developing the HV (10–100 kV) short pulse (50 ns–1 μ s) and a high repetition rate (up to 1 kHz) power supply is to design a reliable and fast HV switch. For this reason, several solutions have been applied, e.g., spark-gap, solid-state, and magnetic switches, or thyratrons.

Spark gaps (triggered or rotating) are frequently used in laboratory experiments as they are cheap and not limited in operating voltage and current. Unfortunately, they have a limited lifetime due to the erosion of electrodes and limited pulse repetition frequency resulting from the necessary recovery of the gap. At an average power of 1 kW, the electrodes have to be forced-cooled by flowing gas.

Solid-state switches based on the serial connection of many elements have been developed during the last few decades. If they operate with a real load in the microsecond range, they will have a very long lifetime. Since the impedance of the streamer and spark discharges differ by several orders of magnitude, there is a danger that if a spark occurs, some elements might be overloaded, broken down, and, consequently, the whole series of elements might be damaged. Last but not least, the price of systems based on solid-state switches is still very high.

Magnetic switches are based on very fast changes in the inductance of a nonlinear inductor with a core made from amorphous metals (i.e., metallic glass). They are very promising as they can operate in the 10 ns range with a repetition frequency in the kHz range and seeing that they contain no moving parts and no discharge. The efficiency of such magnetic switches is from 50–70 %, and within the kW

range of the average power the core requires forced cooling. Such switches, in this case, are also very expensive.

Thyratrons with a cold cathode (modified pseudo-spark discharge) are novel switching elements that can work up to 100 kV producing pulses with a positive or negative polarity, switching 10 kA currents in 10–20 ns with a repetition frequency of 1 kHz. For an operating voltage of up to 50 kV, the cold cathode thyratrons seem to provide switching elements with a sufficiently long lifetime at a reasonable cost.

To illustrate the rich diversity of streamer discharges, Fig. 1 displays three distinct discharge modes observed in a hybrid gas-liquid discharge reactor [5]. The electrode configuration consists of one HV disc electrode made from reticulated vitreous carbon (RVC) placed in the gas phase, with the second HV needle electrode placed in the liquid phase and ground electrode (Fig. 1a). By varying the gap, the HV amplitude and storage capacitor, various streamer modes can be obtained in the gas phase (Figs. 1b–1d).

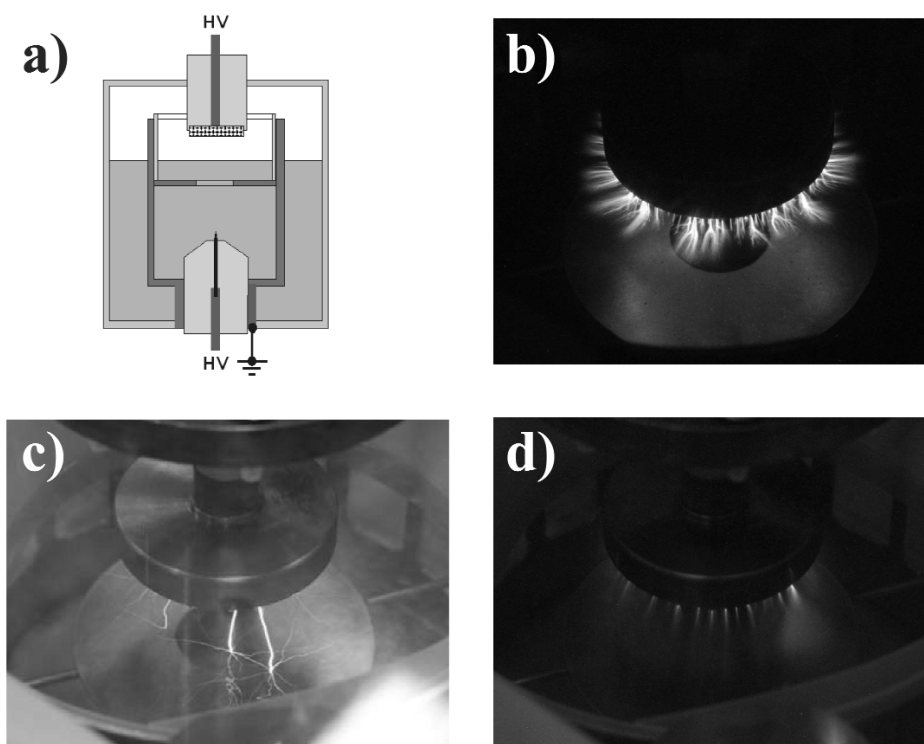


Fig. 1 Hybrid gas-liquid discharge reactor and discharge regimes observed for various combinations of the gap (d), HV pulse amplitude (V), and storage capacitor (C) according to [5]: (a) the electrode geometry schematic; (b) streamer regime for $d = 2.5$ mm, $V = 30$ kV, $C = 7$ nF; (c) streamer regime for $d = 10$ mm, $V = 20$ kV, $C = 7$ nF; and (d) streamer regime for $d = 15$ mm, $V = 30$ kV, $C = 200$ pF.

REACTIVE SPECIES AND STREAMER-INDUCED KINETICS

Depending on a given discharge configuration (electrodes, gas feed composition, and power supply), streamers in N_2 – O_2 mixtures can produce a large variety of reactive species: vibrationally/electronically excited diatomics (e.g., N_2 , O_2 , NO), atomic and molecular positive ions (e.g., N^+ , N_2^+ , N_3^+ , N_4^+ , O^+ , O_2^+ , NO^+), ground-state or electronically excited atomic species (N and O), and negative ions (e.g., O^- , O_2^- , O_3^- , O_4^-) [25–27,43–46]. Some species are formed as a result of electron-impact processes dur-

ing the streamer formation and propagation. Other transient species and stable discharge products appear during the subsequent evolution and decay of the streamer channel in consequence of a variety of recombination, charge-transfer, electron-attachment, and energy-transfer processes, and due to chemical reactions as well. Furthermore, as streamers are by nature repetitive events that may occur at various frequencies starting from a few Hz to frequencies reaching several kHz, the reaction chemistry driven by repetitive streamers may be fundamentally different from the chemistry induced by a single streamer due to the interaction of long-lived species generated and accumulated between consecutive streamers.

Regarding streamer-induced processes in atmospheric gases, numerous experimental and theoretical studies have pointed out the key importance of $N_2(X^1\Sigma^+, \nu)$ and $N_2(A^3\Sigma_u^+)$ molecular, and N/O atomic species [47–54]. Several authors have independently reported $N_2(A^3\Sigma_u^+)$ metastables as a basic source of energy for sustaining UV–vis emissions of OH, NO, NH, and N_2 species observed in various discharges during the post-pulse period [47–51].

Gentile and Kushner [52] performed a computational study of the plasma remediation of N_xO_y from humid air using a repetitively pulsed dielectric barrier discharge (DBD). Reduction ($N + NO \rightarrow N_2 + O$) and oxidation ($NO_2 + OH \rightarrow HNO_3$) channels are confirmed as major removal channels. They found that optimum repetition rates are typically less than hundreds of Hz and that NO can be removed from concentrations of 500 to <1 ppm with an energy cost <70–105 eV/molecule.

The effect of multiple pulses on the plasma chemistry during the remediation of NO_x using DBDs was modeled by Dorai and Kushner [53]. A comparison of the products of single- and multiple-pulse discharge showed marked differences in final concentrations of several products, e.g., NO_2 and HNO_x . The efficiency of NO_x remediation decreased from 240 eV for a single pulse to 185 eV when the same amount of energy was distributed over 20 pulses.

Recently, Zhao et al. [54–56] investigated mechanisms leading to NO_x conversion through a lumped kinetic model and carefully designed experiments. Only N atom radicals appear to be responsible for the NO conversion, and both N atoms and $N_2(A^3\Sigma_u^+)$ metastables appear to be important for NO_2 conversion in nonthermal nitrogen plasmas [55]. Finally, in the presence of oxygen, it is shown that electron-impact dissociation processes producing $O(^3P)$, $N(^4S)$, and $N(^2D)$ species are important for NO_x evolution in N_2 – O_2 mixtures [56]. It is also found that NO formation occurs primarily through $N(^2D) + O_2 \rightarrow NO + O$ reaction.

Ground-state $N_2(X^1\Sigma, \nu)$ species

It is well known that free electrons with energy in the range 1–5 eV efficiently excite the lowest $N_2(X^1\Sigma^+, \nu < 15)$ vibrational levels through electron-vibration (e-V) energy exchange processes. This energy is then apportioned and dissipated in heavy-particle collisions through so-called vibration-vibration (V-V) and vibration-translation (V-T) energy exchanges [43]. The sequence of the e-V, V-V, and V-T processes is capable of creating a significant population of high ground-state vibrational levels, effectively decreasing the threshold for the electron-impact excitation, dissociation and ionization processes.

An inspection of the dynamics of the $N_2(X^1\Sigma_g^+)$ vibrational distribution (VD) by the double-step excitation pulse of electrons representing typical space and time scales of a single streamer was performed in [57]. It was found that due to the order of magnitude of e-V exchange rates with respect to values of V-V and V-T rates, the V-V redistribution and V-T relaxation processes cannot effectively modify the VD on a nanosecond time scale. Consequently, as shown in Fig. 2, the VD evolution is fully determined by e-V exchanges during the streamer propagation, while V-V and V-T exchanges determine the streamer relaxation phase. Such decoupled action of electron-impact and heavy-particle processes is the main reason why the excitation of higher ground-state vibrational levels caused by a single streamer event remains negligible. When the repetition frequency of multiple streamers is high

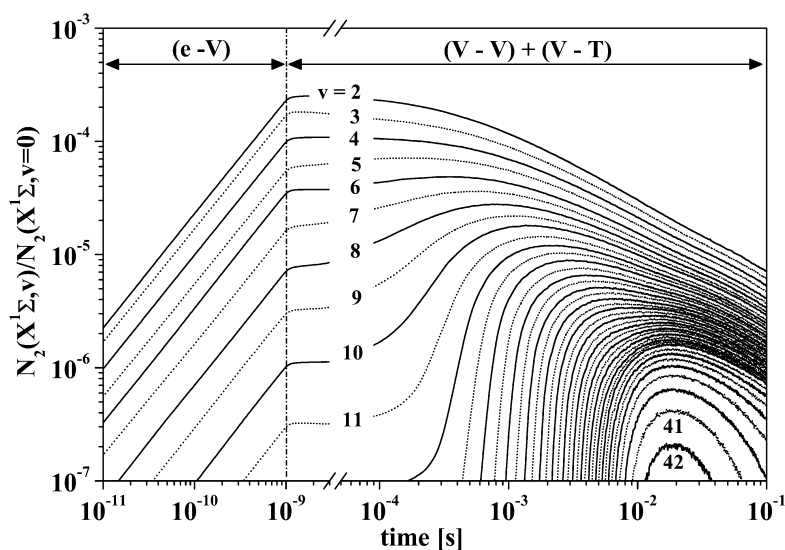


Fig. 2 Model $N_2(X^1\Sigma_g^+)$ vibrational distribution evolution conditioned by the double-step excitation pulse of electrons according to [57] representing typical space and time scales of a single streamer. The typical space and time scales are in this case represented by the duration of the discharge period, which is determined by the characteristic dimension and propagation velocity of the streamer head. For discharge period $\leq 10^{-9}$ [s] the VD evolves predominantly due to e-V exchange, for later times due to V-V and V-T processes.

enough (0.1–1 kHz), the V-T process is unable to quench high vibrational levels between the two consecutive pulses. The accumulation of ground-state species in high- v levels after certain a number of streamer events may possibly then have a direct impact on the discharge characteristics.

Metastable $N_2(A^3\Sigma_u^+)$ species

Metastable $N_2(A^3\Sigma_u^+)$ species are able to dissociate oxygen molecules creating the free oxygen atoms, NO or N_2O . Moreover, due to the reaction with singlet $N_2(a^1\Sigma_u^-)$ metastables, they are even able to produce free electrons. They are therefore assumed to be important during pre-breakdown phases of repetitive discharges and for sustaining an atmospheric pressure glow discharge.

During the lifetime of a single streamer, the $N_2(A^3\Sigma_u^+)$ state is populated by means of several processes. For the period of the discharge (short-pulse or during initial stages), the most important process is the direct electron impact. It populates, together with the $N_2(A^3\Sigma_u^+)$ state, all low-lying N_2 triplet states. As a rule, during the post-discharge, the $N_2(A^3\Sigma_u^+)$ state is formed via an $N(^4S)$ atomic recombination, by an intersystem collisional transfer between the $A^3\Sigma_u^+$, $B^3\Pi_g$, $W^3\Delta$, $B'^3\Sigma_u^-$ states, and through radiative cascades $N_2(D^3\Sigma_u^+, C^3\Pi_u, C'^3\Pi_u, B^3\Sigma_u^-, W^3\Delta) \rightarrow N_2(B^3\Pi_g) + h\nu$ and $N_2(B^3\Pi_g) \rightarrow N_2(A^3\Sigma_u^+, B'^3\Sigma_u^-, W^3\Delta) + h\nu$. The $N_2(A^3\Sigma_u^+)$ therefore serves as a terminal state for a large part of the energy deposited in the N_2 triplet manifold, particularly in pure nitrogen.

Significant quantities of $N_2(A^3\Sigma_u^+)$ species can be anticipated thanks to a couple of unique spectrometric fingerprints that may be easily recognized in the UV–vis–NIR range. To this end, the two groups of energy transfers are essential: resonant energy transfer $N_2(A^3\Sigma_u^+) + AB \rightarrow N_2 + AB^*$ and energy pooling $N_2(A^3\Sigma_u^+) + N_2(A^3\Sigma_u^+) \rightarrow N_2 + N_2^*$ processes [43,47,49–51]. Resonant energy-transfer reactions initiated by the $N_2(A^3\Sigma_u^+)$ excite many diatomic species, typical examples being the transfer with nitric oxide NO or with hydroxyl radical OH. The pooling mechanism then populates several higher N_2 electronic states ($B^3\Pi_g$, $C^3\Pi_u$, $C'^5\Pi_u$, and $C'^3\Pi_u$). There exist two important $N_2(A^3\Sigma_u^+)$ indicators which are based on the energy pooling process: (i) simultaneous occurrence of emissions

through the $N_2(C''^5\Pi_u \rightarrow A'^5\Sigma_g^+)$ Herman infrared (HIR), $N_2(C^3\Pi_u \rightarrow B^3\Pi_g)$ second positive (2.PG), $N_2(C^3\Pi_u \rightarrow B^3\Pi_g)$ Goldstein–Kaplan (GK) and $N_2(B^3\Pi_g \rightarrow A^3\Sigma_u^+)$ first positive (1.PG) systems [49], and (ii) characteristic “hot” vibrational distribution of the $N_2(C^3\Pi_u, v = 0-4)$ electronic state [50]. Fig. 3 shows the typical shape of HIR bands in the 680–820 spectral region arising from $v' = 0-3$ vibronic levels of the $N_2(C''^5\Pi_u)$ state.

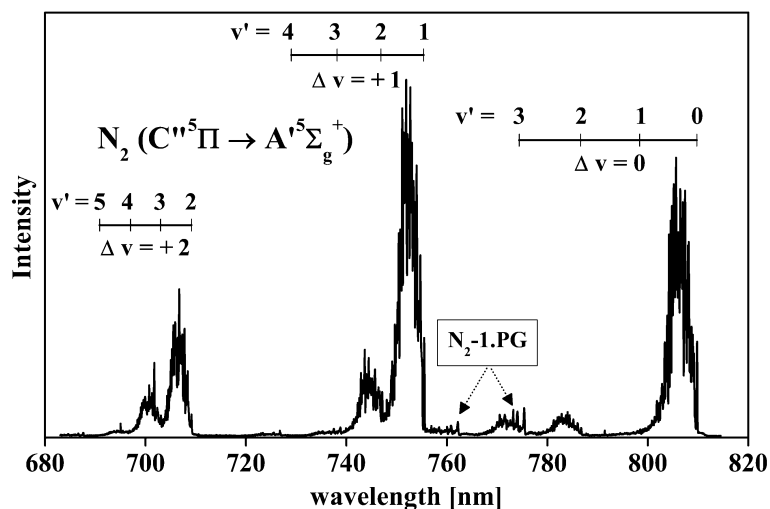


Fig. 3 Characteristic emission of $\Delta v = 0, +1, +2$ sequences of $N_2(C''^5\Pi_u \rightarrow A'^5\Sigma_g^+)$ Herman infrared system induced by $N_2(A^3\Sigma_u^+) + N_2(A^3\Sigma_u^+)$ energy-pooling process in a high-purity nitrogen streamer according to [49]. Two weaker bands indicated by arrows belong to the $\Delta v = +2$ sequence of the N_2 -1.PG system.

Atomic $N(^4S)$ and $O(^3P)$ species

Reactions with the participation of atomic radicals initiate the removal of a number of atmospheric pollutants, e.g., nitrogen oxides, sulfur oxides, carbon monoxide, methane, and volatile organic compounds. Atomic nitrogen and oxygen are formed through (i) direct electron-impact dissociation of parent N_2 , O_2 , and NO molecules by energetic streamer head electrons, (ii) dissociative recombination of N_2^+ , O_2^+ , and NO^+ ions, (iii) various ion conversion processes, and (iv) chemical reactions [17].

The presence of nitrogen atoms may be manifested through streamer-induced emission in two basic ways [17,47]. Firstly, it is well known that two recombining $N(^4S)$ atoms directly populate one of $N_2(X^1\Sigma, A^3\Sigma, A^5\Sigma)$ states. The energy of $N_2(A^5\Sigma)$ species is then transferred collisionally to the $N_2(B^3\Pi_g)$ state and, consequently, radiation through the N_2 -1.PG system occurs. Because recombining nitrogen atoms can indirectly produce the 1.PG emission, its intensity with the characteristic enhancement of the $N_2(B^3\Pi_g, v' = 10-12)$ level intensities is often used as a $N(^4S)$ marker. Secondly, nitrogen and oxygen atoms can recombine through $N + O + M \rightarrow M + NO(A^2\Sigma, B^2\Pi, C^2\Pi)$ to form electronically excited nitric oxide. Simultaneous formation of the $A^2\Sigma, B^2\Pi$, and $C^2\Pi$ states will result in the simultaneous generation of $NO-\gamma, NO-\beta$, and $NO-\delta$ systems, respectively. The intensity of the $NO-\beta$ emission can be conveniently used as an indicator of the $N(^4S)$.

DETERMINATION OF REACTIVE SPECIES

In an attempt to get a deeper insight into species produced by streamers, several diagnostic approaches based on optical techniques have been applied recently and their continuing development may help to

investigate streamer basics. What holds promise for the future are laser-based methods and techniques based on energy-transfer processes.

Laser-based techniques

Diagnostic approaches based on tunable short-pulse lasers, e.g., LIF (laser-induced fluorescence), OODR-LIF (optical-optical double resonance-LIF), TALIF (two-photon absorption laser-induced fluorescence), LA (laser absorption), and CARS (coherent anti-Stokes Raman scattering), can offer qualities which are necessary to diagnose environments conditioned by propagating or decaying streamers: both spatial and temporal resolutions, together with high sensitivity [58–62].

LIF and $N_2(A^3\Sigma)$, NO and OH species

The LIF spectroscopy with single-photon excitation provides direct access to ground-state NO($X^2\Pi$), OH($X^2\Pi$), and metastable $N_2(A^3\Sigma)$ populations. Concerning $N_2(A^3\Sigma)$ species, the LIF method uses a dipole-allowed transition between $A^3\Sigma_u^+ \leftrightarrow B^3\Pi_g$ states. The standard approach [63] typically uses $\lambda = 550\text{--}620$ nm photons to pump the upper $B^3\Pi_g$ state via the $\Delta v = 4$ sequence, the fluorescence through $\Delta v = 3$ or 2 transitions is followed in the 640–780 nm spectral range. As the radiative lifetime of the $B^3\Pi_g$ state is relatively long ($\sim 4\text{--}10$ μs) while the quenching rate constant by N_2 is quite high ($\sim 5 \times 10^{-11}$ $\text{cm}^3 \text{s}^{-1}$), the fluorescence signal is, unfortunately, considerably attenuated due to efficient collisional quenching.

In connection with both NO($X^2\Pi$) and OH($X^2\Pi$) species, the LIF technique employs UV photons to excite and detect the doublet $X^2\Pi \leftrightarrow A^2\Sigma$ transition. Roth and Gundersen [64] reported one of the first attempts to determine NO destruction in a single streamer. They studied 2-D LIF images of NO distribution after a needle-plane pulsed negative corona discharge in the air seeded with NO (25 ppm). The images were acquired by exciting (0,0) band at 226 nm with fluorescence detection through a narrow band-pass filter, centered at 253 nm. Both laser and discharge were synchronized and operated at 10 Hz, and nearly uniform NO destruction throughout most of the streamer region was reported.

A similar study was performed in the case of a N_2 –NO mixture by Hazama et al. [65]. They observed the NO removal process along an individual streamer employing single-shot LIF images. NO removal is explained on the basis of N atoms produced by energetic electrons. Kanazawa et al. [66] investigated 2-D LIF density profiles of NO in the case of DC corona driven in air +200 ppm NO mixture. LIF images discovered NO removal also in the upstream region of the reactor.

Ono and Oda [67] studied hydroxyl radicals produced in a needle-plate pulsed positive corona discharge in a N_2 – O_2 – H_2O mixture. The 2-D LIF images from a 16-mm discharge gap were acquired by exciting a (3,0) band at 248 nm with fluorescence detection through the (3,2) band at 297 nm. The decay profiles of OH radicals were obtained, and density was estimated using a three-level model.

OODR-LIF and $N_2(A^3\Sigma)$

The fluorescence yield provided by a standard single-photon LIF on the $N_2(A^3\Sigma)$ drops significantly with increasing gas pressure because of collisional quenching of the $B^3\Pi_g$ state. Additionally, such a fluorescence signal can easily be affected both by scattered laser light and by emission produced by a discharge. Dilecce et al. [68] proposed using an alternative OODR-LIF method at an atmospheric pressure to overcome this limitation. The OODR scheme in principle requires two tunable lasers in a pump-probe configuration to detect $N_2(A^3\Sigma)$ through $A^3\Sigma_u^+ \rightarrow B^3\Pi_g \rightarrow C^3\Pi_u$ transitions. As demonstrated in [68], the double laser excitation can be achieved by a single laser set-up. Dilecce et al. [68] also tested the OODR sensitivity with respect to conventional single-photon LIF for intermediate pressures (up to 300 Torr) in a pulsed point-plate RF discharge. At atmospheric pressure, a significant increase of OODR sensitivity over conventional LIF (close to two orders of magnitude) is predicted.

Laser absorption and O₃

Ono and Oda [69] investigated spatial distribution of ozone density by 2-D LA at 248 nm in a pulsed multiple needle-to-plane corona discharge in dry air. After passing through the reactor, the laser beam was projected onto a fluorescent glass plate and the resulting beam pattern was observed with an ICCD detector. By studying temporal variations of the ozone density distribution after the discharge pulse, it was implied that most of the ozone is probably produced by a secondary streamer.

TALIF and atomic N(⁴S) and O(³P) species

The TALIF technique has become a standard for detecting both N and O ground-state atomic species. The TALIF is based on the absorption of two UV photons, and its great advantage is a large spectral separation between the UV laser and fluorescence photons [62].

With reference to N(⁴S) atoms, the measurement can be carried out employing the two different excitation-detection pathways. The absorption of two UV photons with $\lambda = 206.7$ nm through the $2p^3\ ^4S^0 \rightarrow 3p^4S^0_{J=3/2}$ transition induces the fluorescence via the $3p^4S^0_{J=3/2} \rightarrow 3s^4P$ transition at $\lambda = 746.8$ nm. Alternatively, the absorption of two $\lambda = 210.8$ nm photons through the $2p^3\ ^4S^0 \rightarrow 3s\ ^4D^0_{J=7/2}$ transition induces the fluorescence via $3s\ ^4D^0_{J=7/2} \rightarrow 3s\ ^4P_{J=5/2}$ transition at $\lambda = 868$ nm. Lukas et al. [70] used the first of the two pathways to measure space- and time-resolved relative N(⁴S) density distributions at a single filament in a pulsed pin-to-plate DBD in N₂ and in N₂ + O₂ mixture.

The TALIF scheme on O(³P) atoms utilizes the absorption of two $\lambda = 225.6$ nm photons through the $2p^3P_2 \rightarrow 3p^3P_2$ transition followed by the fluorescence via the $3p^3P_2 \rightarrow 3s\ ^3S_1$ transition at $\lambda = 844.6$ nm. Ono et al. [71] investigated O(³P) production in a pulsed needle-to-plane DBD in a dry or humid N₂ + O₂ mixture. In their case, the TALIF signal had to be corrected for a contribution given by the O₂ photodissociation caused by a focused laser beam. It was shown that the decay rate of atomic oxygen increases linearly with both O₂ concentration and humidity.

Techniques based on energy-transfer processes

While laser-based techniques utilize interaction of external photons with probed species, techniques based on energy-transfer processes make use of elementary processes capable of linking probed species with electronically excited reference species that are readily observable in emission.

Herman infrared emission and N₂(A³Σ) species

With regard to N₂(A³Σ) metastables, a new method based on pooling and resonant energy transfer was developed recently [63] and it was tested [64] to investigate streamers in pure nitrogen. Essentially, the method of “normalized HIR curves” tracks the evolution of N₂(A³Σ_u⁺) species through the square root of the HIR emission intensity. The relative N₂(A³Σ_u⁺) time-course is then placed on an absolute scale by applying a proper normalizing procedure [63].

Energy levels and transitions involved in the method are schematically shown in Fig. 4a. It has been demonstrated [64] that in pure nitrogen streamers generated in wire-cylinder geometry the aggregate N₂(A³Σ_u⁺) concentrations in the two lowest $\nu = 0, 1$ vibrational levels reach as much as $\sim 5 \times 10^{14}$ [cm⁻³]. Former density levels were fixed close to the central wire anode during the early post-discharge time (~ 1 μs). Figure 4b shows the evolution N₂(A³Σ_u⁺, $\nu = 0-1$) species in decaying, high-purity nitrogen streamer. Considering that HIR emission has been observed apparently only in connection with the pooling, it provides an interesting tool whenever the pooling mechanism becomes a predominant N₂(A³Σ_u⁺) self-quenching process.

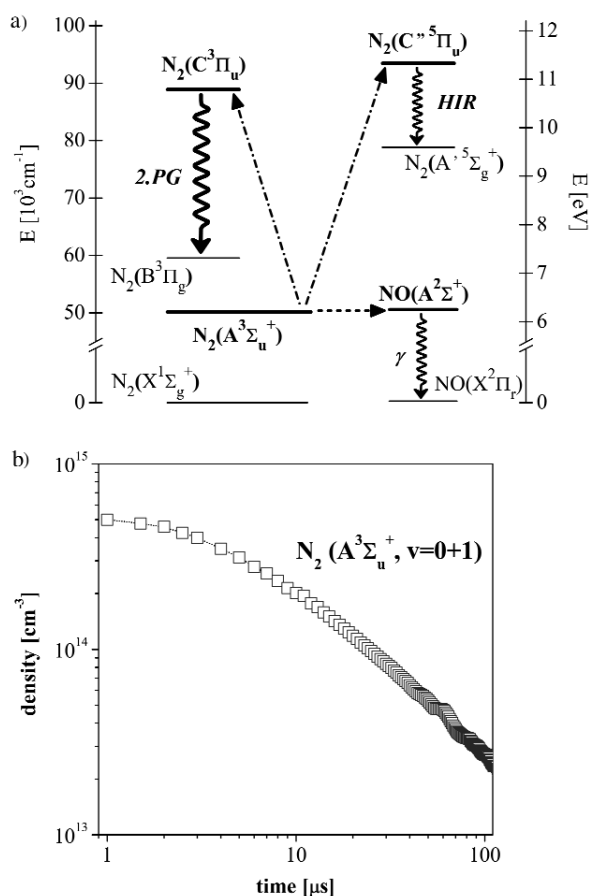


Fig. 4 Determination of $N_2(A^3\Sigma_u^+)$ density: (a) simplified scheme of crucial energy levels and collisional/radiative transitions used in the method of “normalized HIR curves” and (b) evolution of density of $N_2(A^3\Sigma_u^+, \nu = 0-1)$ species in decaying, high-purity nitrogen streamer.

Pooling and $N_2(B^3\Pi, C^3\Pi, C'^5\Pi)$ species

The fact the pooling process populates several higher electronically excited states offers an interesting opportunity to fix the densities of those states. In [74], it is demonstrated that a $N_2(C^3\Pi_u)$ concentration can be evaluated from a $N_2(A^3\Sigma_u^+)$ state concentration when the two basic $N_2(C^3\Pi_u)$ state excitation processes, i.e., electron impact and pooling, are not effective simultaneously. This is certainly true in the case of nitrogen streamers: the electron impact controls the $N_2(C^3\Pi_u)$ state population during the streamer propagation while the pooling controls the post-discharge period [50]. Figure 5 shows the corresponding evolution of the $N_2(C^3\Pi_u, \nu = 0-4)$ concentration in a high-purity nitrogen streamer. In principle, a similar approach might be applied to determine densities of $N_2(B^3\Pi_g)$ and $N_2(C'^5\Pi_u)$ species as well. However, with regard to the $N_2(B^3\Pi_g)$ state a much more complex model [75] reflecting an intersystem collisional transfer between the $A^3\Sigma_u^+$, $B^3\Pi_g$, $W^3\Delta$, $B'^3\Sigma_u^-$ states is necessary. Concerning the $N_2(C'^5\Pi_u)$ state, basic data such as reliable values for both radiative and collisional quenching are, unfortunately, not available.

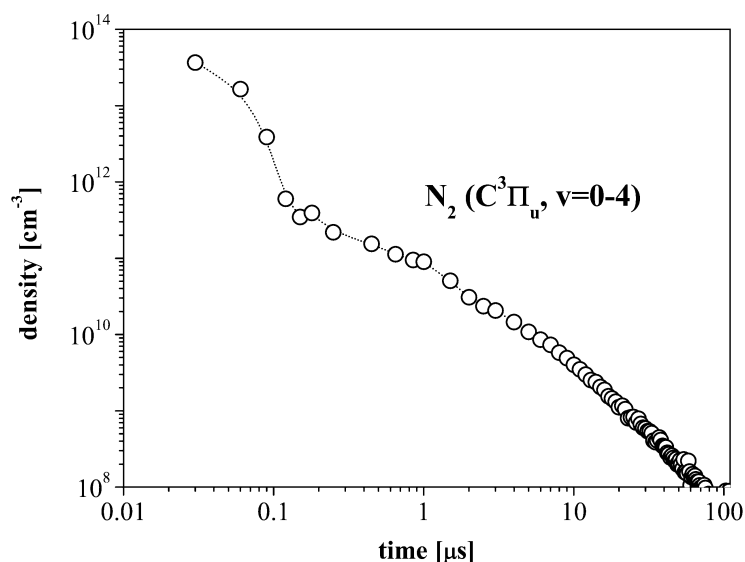


Fig. 5 Dynamics of density of $N_2(C^3\Pi_u, v = 0-4)$ species in high-purity nitrogen streamer as set forth in [74]. Evaluated from $N_2(A^3\Sigma_u^+)$ density by assuming the $N_2(A^3\Sigma_u^+) + N_2(A^3\Sigma_u^+)$ energy-pooling process as an exclusive source of $N_2(C^3\Pi_u)$ state excitation during the streamer decay period.

Resonant energy transfer and NO and OH species

The presence of $N_2(A^3\Sigma_u^+)$ metastables was shown to be essential for exploring the dynamics of NO and OH formation in nitrogen streamers. Efficient excitation of $OH(A^2\Sigma^+)$ and $NO(A^2\Sigma^+)$ states through resonant energy transfer of $N_2(A^3\Sigma_u^+)$ energy may have very important implications for the further improvement of quantitative OH/NO measurements in environments where the use of laser-based techniques appears to be limited. In [76], the quantitative determination of OH density comes from the demonstration that both $OH(X^2\Pi)$ and $NO(X^2\Pi)$ species are probed simultaneously by the $N_2(A^3\Sigma_u^+)$ species and the $NO(X^2\Pi)/OH(X^2\Pi)$ density ratio is proportional to the ratio of $NO(A^2\Sigma^+)$ and $OH(A^2\Sigma^+)$ emission intensities. The OH production was studied for H_2O admixtures up to 2000 PPM and the highest density of OH species ($\sim 10^{14} \text{ cm}^{-3}$) was fixed during early afterglow for the $N_2 + 500 H_2O$ PPM mixture.

CONCLUSIONS

The production of several specific atomic and molecular species appears to be essential for the reaction chemistry of filamentary streamers in atmospheric gases. The need of relevant experimental data has recently triggered a number of diagnostic studies focusing on dynamics of N_2 , OH, NO, O_3 molecular, and N and O atomic species. Basic small-space and short time scales of propagating streamers, conditioned by collisional processes occurring at high pressures in a high self-consistent electric field in the streamer head, impose considerable requirements on diagnostic techniques. Applied diagnostic techniques were based either on tunable pulsed lasers or on specific energy-transfer processes. In several cases, fixed absolute densities of reactive species have been reported. Despite major drawbacks of both groups, i.e., severe quenching of the fluorescence state in the case of LIF/TALIF/OODR techniques and rate constant dependence in the case of energy-transfer methods, all reported results show evidence of great potential. Further progress might be made by applying diagnostic approaches developed in various laboratories to investigate a well-defined reference streamer discharge.

ACKNOWLEDGMENTS

This work was supported by the Grant Agency of the Academy of Sciences of the Czech Republic under contract No. A1043403. The authors would like to thank John A. Novotny for helpful comments and review of the manuscript.

REFERENCES

1. H. Raether. *Electron Avalanches and Breakdown in Gases*, Butterworths, London (1964).
2. A. N. Lagarkov, I. M. Rutkevich. *Ionization Waves in Electrical Breakdown of Gases*, Springer Verlag, New York (1986).
3. Yu. P. Raizer. *Gas Discharge Physics*, Springer Verlag, Berlin (1997).
4. A. Fridman, A. Chirokov, A. Gutsol. *J. Phys. D: Appl. Phys.* **38**, R1 (2005).
5. P. Lukeš, M. Člupek, V. Babický, V. Janda, P. Šunka. *J. Phys. D: Appl. Phys.* **38**, 409 (2005).
6. P. Šunka, V. Babický, M. Člupek, P. Lukeš, M. Šimek, J. Schmidt, M. Cernák. *Plasma Sources Sci. Technol.* **8**, 258 (1999).
7. P. E. Frayssines, O. Lesaint, N. Bonifaci, A. Denat, F. Devaux. *IEEE Trans. Dielect. Elect. Insul.* **10**, 970 (2003).
8. B. M. Penetrante, J. N. Bardsley, M. C. Hsiao. *Jpn. J. Appl. Phys., Pt. 1* **36**, 5007 (1997).
9. B. M. Penetrante, M. C. Hsiao, J. N. Bardsley, B. T. Merritt, G. E. Vogtlin, A. Kuthi, C. P. Burkhart, J. R. Bayeless. *Plasma Sources Sci. Technol.* **6**, 251 (1997).
10. B. M. Penetrante, R. M. Brusasco, B. T. Merritt, G. E. Vogtlin. *Pure Appl. Chem.* **71**, 1829 (1999).
11. R. Hackam, H. Akiyama. *IEEE Trans. Dielect. Elect. Insul.* **7**, 654 (2000).
12. K. Yan, E. J. M. van Heesch, A. J. M. Pemen, P. A. H. J. Huijbrechts. *Plasma Chem. Plasma Process.* **21**, 107 (2001).
13. H. H. Kim. *Plasma Process. Polym.* **1**, 91 (2004).
14. W. J. M. Samaranayake, Y. Miyahara, T. Namihira, S. Katsuki, T. Sakugawa, R. Hackam, H. Akiyama. *IEEE Trans. Dielect. Elect. Insul.* **7**, 254 (2000).
15. M. Šimek, M. Člupek. *J. Phys. D: Appl. Phys.* **35**, 1171 (2002).
16. R. Ono, T. Oda. *J. Adv. Oxid. Technol.* **8**, 167 (2005).
17. I. A. Kosnyi, A. Yu. Kostinsky, A. A. Matveyev, V. P. Silakov. *Plasma Sources Sci. Technol.* **1**, 207 (1992).
18. A. A. Matveyev, V. P. Silakov. *Plasma Sources Sci. Technol.* **8**, 162 (1999).
19. J. T. Herron. *J. Phys. Chem. Ref. Data* **28**, 1453 (1999).
20. L. W. Sieck, J. T. Herron, D. S. Green. *Plasma Chem. Plasma Process.* **20**, 235 (2000).
21. J. T. Herron, D. S. Green. *Plasma Chem. Plasma Process.* **21**, 459 (2001).
22. I. Gallimberti. *J. Phys. D: Appl. Phys.* **5**, 2179 (1972).
23. A. Deryugin, A. Napartovich, C. Gorse, F. Paniccia, M. Capitelli. *Plasma Chem. Plasma Process.* **17**, 79 (1997).
24. G. V. Naidis. *J. Phys. D: Appl. Phys.* **30**, 1214 (1997).
25. F. Tochikubo, H. Arai. *Jpn. J. Appl. Phys., Pt. 1* **41**, 844 (2002).
26. O. Eichwald, N. A. Guntoro, M. Yousfi, M. Benhenni. *J. Phys. D: Appl. Phys.* **35**, 439 (2002).
27. R. Barni, P. Esena, C. Riccardi. *J. Appl. Phys.* **97**, 073301 (2005).
28. I. Gallimberti, J. K. Hepworth, R. C. Klewe. *J. Phys. D: Appl. Phys.* **7**, 880 (1974).
29. P. Stritzke, I. Sander, H. Raether. *J. Phys. D: Appl. Phys.* **10**, 2285 (1977).
30. W. J. Yi, P. F. Williams. *J. Phys. D: Appl. Phys.* **35**, 205 (2002).
31. P. E. Frayssines, N. Bonifaci, A. Denat, O. Lesaint. *J. Phys. D: Appl. Phys.* **35**, 369 (2002).
32. E. M. van Veldhuizen, W. R. Rutgers. *J. Phys. D: Appl. Phys.* **35**, 2169 (2002).
33. P. Tardiveau, E. Marode, A. Agneray. *J. Phys. D: Appl. Phys.* **35**, 2823 (2002).

34. T. Namihira, D. Y. Wang, S. Katsuki, R. Hackam, H. Akiyama. *IEEE Trans. Plasma Sci.* **31**, 1091 (2003).
35. R. Ono, T. Oda. *Jpn. J. Appl. Phys., Pt. 1* **43**, 321 (2004).
36. A. A. Kulikovskiy. *J. Phys. D: Appl. Phys.* **33**, 1514 (2000).
37. S. V. Pancheshnyi, S. M. Starikovskaia, A. Yu. Starikovskii. *J. Phys. D: Appl. Phys.* **34**, 105 (2001).
38. S. Pancheshnyi. *Plasma Sources Sci. Technol.* **14**, 645 (2005).
39. I. A. Kossyi, V. P. Silakov. *Plasma Sources Sci. Technol.* **14**, 594 (2005).
40. K. Yan. Ph.D. dissertation, Technische Universiteit Eindhoven, Eindhoven (2001).
41. E. Kuffel, W. S. Zaengl, J. Kuffel. *High Voltage Engineering: Fundamentals*, Newnes, Oxford (2004).
42. J. Mankowski, M. Kristiansen. *IEEE Trans. Plasma Sci.* **28**, 102 (2000).
43. M. Capitelli, C. M. Ferreira, B. F. Gordiets, A. I. Osipov. *Plasma Kinetics in Atmospheric Gases*, Springer Verlag, New York (1997).
44. A. A. Kulikovskiy. *IEEE Trans. Plasma Sci.* **25**, 439 (1997).
45. A. A. Kulikovskiy. *IEEE Trans. Plasma Sci.* **26**, 1339 (1998).
46. A. A. Kulikovskiy. *IEEE Trans. Plasma Sci.* **29**, 313 (2001).
47. M. Šimek, V. Babický, M. Člupek, S. Debenedictis, G. Dilecce, P. Šunka. *J. Phys. D: Appl. Phys.* **31**, 2591 (1998).
48. F. Tochikubo, T. H. Teich. *Jpn. J. Appl. Phys., Pt. 1* **39**, 1343 (2000).
49. M. Šimek, V. Babický, M. Člupek, P. Šunka. *J. Phys. D: Appl. Phys.* **34**, 3185 (2001).
50. M. Šimek, S. Debenedictis, G. Dilecce, V. Babický, M. Člupek, P. Šunka. *J. Phys. D: Appl. Phys.* **35**, 1981 (2002).
51. R. Ono, T. Oda. *J. Appl. Phys.* **97**, 013302 (2005).
52. A. C. Gentile, M. J. Kushner. *J. Appl. Phys.* **78**, 2074 (1995).
53. R. Dorai, M. J. Kushner. *J. Phys. D: Appl. Phys.* **34**, 574 (2001).
54. G. B. Zhao, X. Hu, M. C. Yeung, O. A. Plumb, M. Radosz. *Ind. Eng. Chem. Res.* **43**, 2315 (2004).
55. G. B. Zhao, X. Hu, M. D. Argyle, M. Radosz. *Ind. Eng. Chem. Res.* **43**, 5077 (2004).
56. G. B. Zhao, S. V. B. J. Garikipati, X. Hu, M. D. Argyle, M. Radosz. *AIChE J.* **51**, 1800 (2005).
57. M. Šimek. *J. Phys. D: Appl. Phys.* **35**, 1967 (2002).
58. W. Demtröder. *Laser Spectroscopy: Basic Concepts and Instrumentation*, Springer Verlag, Berlin (2003).
59. S. Debenedictis, G. Dilecce. *Pure Appl. Chem.* **74**, 317 (2002).
60. G. Dilecce, P. F. Ambrico, M. Šimek, S. Debenedictis. *App. Phys. B* **75**, 131 (2002).
61. K. Niemi, V. Schulz-von der Gathen, H. F. Döbele. *J. Phys. D: Appl. Phys.* **34**, 2330 (2001).
62. H. F. Döbele, T. Mosbach, K. Niemi, V. Schulz-von der Gathen. *Plasma Sources Sci. Technol.* **14**, S31 (2005).
63. S. Debenedictis, G. Dilecce, M. Šimek. *J. Phys. D: Appl. Phys.* **31**, 1197 (1998).
64. G. J. Roth, M. A. Gundersen. *IEEE Trans. Plasma Sci.* **27**, 28 (1999).
65. H. Hazama, M. Fujiwara, M. Tanimoto. *Chem. Phys. Lett.* **323**, 542 (2000).
66. S. Kanazawa, Y. Shuto, N. Sato, T. Ohkubo, Y. Nomoto, J. Mizeraczyk, J. S. Chang. *IEEE Trans. Ind. Appl.* **39**, 333 (2003).
67. R. Ono, T. Oda. *J. Phys. D: Appl. Phys.* **35**, 2133 (2002).
68. G. Dilecce, P. F. Ambrico, S. Debenedictis. *Plasma Sources Sci. Technol.* **14**, 561 (2005).
69. R. Ono, T. Oda. *J. Phys. D: Appl. Phys.* **37**, 730 (2004).
70. C. Lukas, M. Spaan, V. Schulz-von der Gathen, M. Thomson, R. Wegst, H. F. Döbele, M. Neiger. *Plasma Sources Sci. Technol.* **10**, 445 (2001).
71. R. Ono, Y. Yamashita, K. Takezawa, T. Oda. *J. Phys. D: Appl. Phys.* **38**, 2812 (2005).
72. M. Šimek. *Plasma Sources Sci. Technol.* **12**, 421 (2003).
73. M. Šimek. *Plasma Sources Sci. Technol.* **12**, 454 (2003).

74. M. Šimek. *Proceedings of the 18th European Conference on the Atomic and Molecular Physics of Ionised Gases*, Lecce, Italy (2006).
75. S. Debenedictis, G. Dilecce, M. Šimek. *J. Chem. Phys.* **110**, 2947 (1999).
76. M. Šimek. *Proceedings of the XVth International Conference on Gas Discharges and Their Applications*, Vol. 2, Toulouse, France, pp. 853–856 (2004).